Reversible Na-Ion Uptake in Si Nanoparticles

Xu, Y; Swaans, E; Basak, S; Zandbergen, HW; Borsa, DM; Mulder, FM

DOI
10.1002/aenm.201501436

Publication date
2016

Document Version
Final published version

Published in
Advanced Energy Materials

Reversible Na-Ion Uptake in Si Nanoparticles

*Yaolin Xu, Ellie Swaans, Shibabrata Basak, Henny W. Zandbergen, Dana M. Borsa, and Fokko M. Mulder**

Na ion batteries attract significant research interest since they provide potentially high energy density while using low cost and abundant sodium as the active ion.[1–5] Due to the analogy between Li and Na ions, different types of materials that have been applied in Li-ion batteries are also studied for application in Na ion batteries and vice versa.[6–9] Si has been extensively investigated since it has high theoretical lithiation capacity up to $Li_{4.4}Si$.[10–12] In general, the sodiation of Si is anticipated to be different with respect to phase behavior, insertion voltages, and kinetic barriers when compared to Li ion, for instance, because of the difference in ionic radius of Na^+ (0.97 Å) and Li^+ (0.68 Å).[13,14] From thermal synthesis of Na—Si materials it is known that NaSi is the most Na rich phase for Na—Si binary compounds,[15] which would enable a sizeable capacity of 954 mAh g^{-1} and be promising for Na-ion battery anodes.

Electrochemical sodiation of Si has been studied theoretically;[14,16–20] micrometer-sized Si[21] and nanosized Si (100 nm)[22] also have been studied in experiments but until now reversible sodium insertion has remained unsuccessful. Anticipating that nanoscaling is of advantage for the kinetics of ion insertion and extraction,[23,24] and considering the fact that amorphous Si is more favorable for Na insertion,[17,20] we studied Si particles with much reduced size (≈20 nm) containing a large fraction of amorphous Si obtained from expanding thermal plasma chemical vapor deposition (ETPCVD) of silane. The work presented here reports that, to our knowledge for the first time, reversible electrochemical Na ion uptake in Si is experimentally achieved for a significant capacity.

The morphology of Si nanoparticles (NPs) produced by ETPCVD are characterized with scanning electron microscopy (SEM) and high-resolution transmission electron microscopy (TEM). **Figure 1**a shows that bundles of Si nanoparticle clusters are observed in a fibrous, tree like, morphology with micrometer sized fiber branches consisting of small nanoparticles. Figure 1b demonstrates that individual crystalline Si particles appear to be nicely spherical, whereas the surface layer has been oxidized. A native oxidation layer grows on the surface of individual Si nanoparticles when they are exposed to traces of air after synthesis. The presence of such limited pacifying oxide layer appeared of advantage for the further processing in air. The average thickness of the oxidation layer is around 1.2 nm, and it is amorphous when observed by X-ray diffraction (XRD) (Figure 1c), i.e., only peaks corresponding to crystalline Si are visible. For a particle with a size of 20 nm Si in diameter and 1.2 nm outer layer of SiO_2, the volume percentage of SiO_2 is 28.8%. Raman spectra (Figure 1d) on the sample report that both crystalline and amorphous Si exist and the amount of amorphous Si is significant (c-Si:a-Si = 0.39:0.61; quantitative analysis in the Supporting Information). To determine the amount of oxygen in the sample, thermogravimetric analysis (TGA) is carried out by heating the Si NP sample under a mixture of O_2/Ar gas and fully oxidizing Si into SiO_2. The result indicates that the amount of Si accounts for 69.0 wt% of the sample (Figure S2, Supporting Information), i.e., $Si:SiO_2$ = 0.83:0.17 in mole. Meanwhile, the volume fraction from the estimated mass ratio above is 28.2% and is in good quantitative agreement with the one estimated from TEM.

Galvanostatic tests on the Si NP electrode are performed using different dis-/charge currents between applied potentials of 0.01 and 2.8 V. In this paper, all specific currents applied are calculated with respect to the mass of Si. De-/sodiation capacities of Si stated in this paper are the capacities after subtracting the capacity of the super P carbon black (Figure S3, Supporting Information), and excluding inactive SiO_x inside the sample.

Figure 2a demonstrates an initial sodiation capacity of 1027 mAh g^{-1} for Si at 20 mA g^{-1}, which is higher than the theoretical capacity (954 mAh g^{-1} for NaSi). A large part of this initial capacity is attributed to the irreversible formation of a solid electrolyte interface (SEI) layer on the surface of Si in combination with some decomposition of electrolyte, and possibly also the irreversible formation of sodium silicate from reaction with SiO_2. The subsequent Na ion extraction process achieves a capacity up to 270 mAh g^{-1}, indicating that a significant Na fraction is stored reversibly, next to the large irreversible part. For the subsequent few cycles the sodiation capacity decreases from above 410 mAh g^{-1} to around 300 mAh g^{-1} but the desodiation capacity is relatively stable around 260 mAh g^{-1}. The Coulombic efficiency grows gradually to >90%, after which the de-/sodiation capacity becomes relatively stable. After 100 cycles the reversible capacity retention reaches 248 mAh g^{-1}, which is 92% of the first desodiation capacity; and the Coulombic efficiency declines slowly to 87% in this cycle test. Additionally, Figure 1e shows that after charge/discharge for 100 cycles Si particles in this electrode got fractured into small grains and no crystalline phase is observed.

Y. Xu, Prof. F. M. Mulder
Materials for Energy Conversion and Storage (MECS)
Department of Chemical Engineering
Delft University of Technology
Julianalaan 136, 2628 BL, Delft, The Netherlands
E-mail: F.M.Mulder@tudelft.nl
E. Swaans, Dr. D. M. Borsa
Roth and Rau B. V.
Luchthavenweg 10, 5657 EB, Eindhoven, The Netherlands
S. Basak, Prof. H. W. Zandbergen
Kavli Institute of Nanoscience
Delft University of Technology
Lorentzweg 1, 2628 CJ, Delft, The Netherlands

DOI: 10.1002/aenm.201501436

ADVANCED ENERGY MATERIALS
www.advenergymat.de

www.MaterialsViews.com

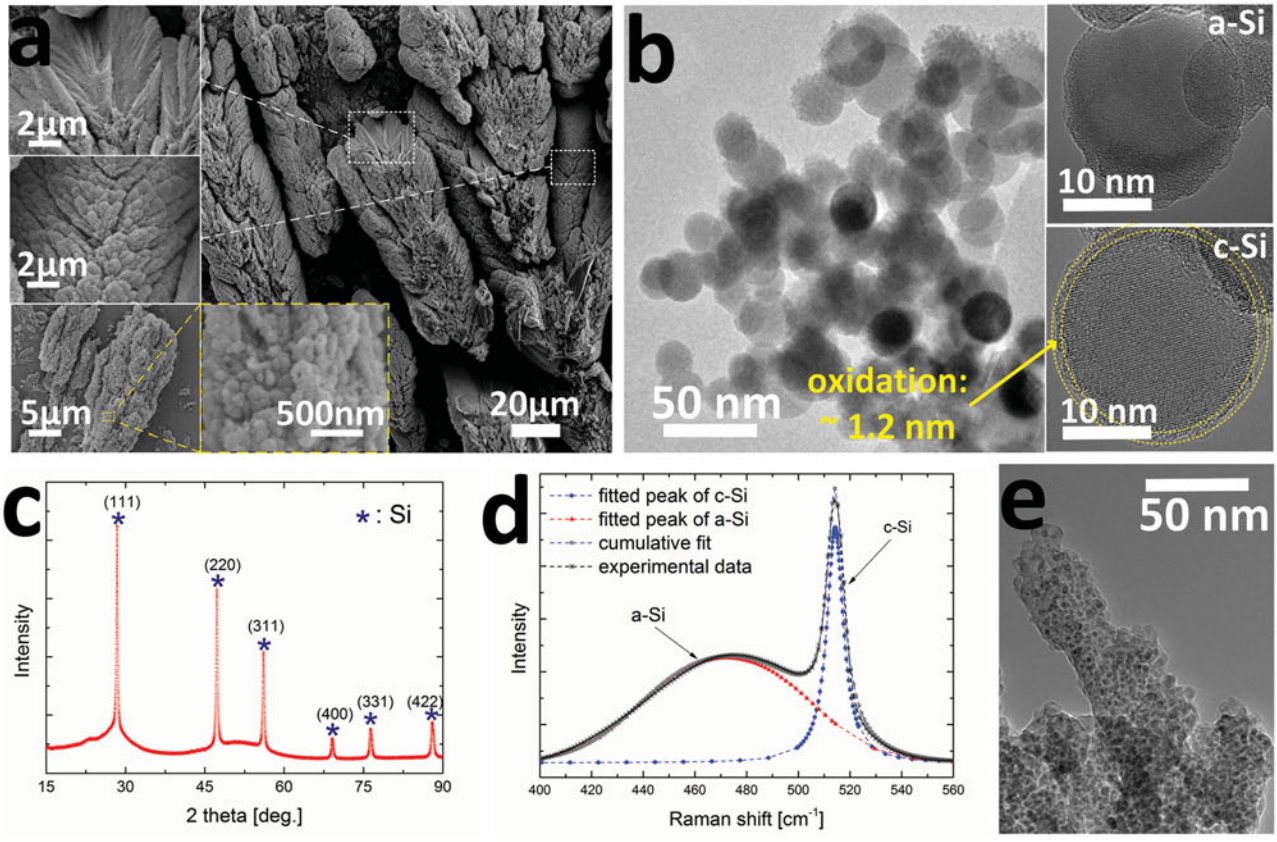

Figure 1. a) SEM of Si nanoparticle clusters. b) TEM of Si nanoparticles. c) X-ray diffraction patterns on as-synthesized Si nanoparticles. d) Raman spectroscopy of Si nanoparticles showing the coexistence of a-Si and c-Si. e) Morphology of sodiated Si NP electrode after charge/discharge for 100 cycles at 20 mA g^{-1}.

The galvanostatic sodiation voltage profile (Figure 2b) demonstrates a higher voltage plateau at ≈1.1 V for the first Na insertion process, attributed to the SEI formation and side reactions with SiO_x; while this is not visible for the following cycles. A long sloping lower voltage plateau is observed during which most sodium is inserted into Si. In comparison, during desodiation the voltage pattern shows a more continuous increase from 0.1 V to the cut-off voltage. In terms of the energy efficiency the higher voltages during desodiation are not favorable.

The Si NP electrode is also cycled at a varying current range from 10 to 500 mA g^{-1}. Figure 2c shows that an initial reversible desodiation capacity of 279 mAh g^{-1}, corresponding to $Na_{0.29}Si$, is achieved at 10 mA g^{-1}. At the higher cycling rates the capacity appears to be reaching lower values, but at the highest dis-/charge rate there is still a capacity retention of 90 mAh g^{-1}. Meanwhile the Coulombic efficiency appears to grow with increasing current rates, and an efficiency of >98% is achieved at 500 mA g^{-1}. Higher current rate probably mainly leads to a surface layer reaction of Si avoiding deeper Na ion diffusion into the particles. This reduces the ionic transport time and accelerates the desodiation kinetics; hence, a higher Coulombic efficiency can be achieved at relatively high rates.

Figure 2d shows that the overpotentials resulting from higher current rates are rather symmetrical for both Na insertion and extraction. The electronic and ionic resistances in the system make that the cut-off voltages are reached more rapidly at higher rates, hence the achieved capacity reduces. Still in Figure 2c it is visible that increasing dis-/charge rates is possible with lower capacity but with improved Coulombic efficiency. Apart from sufficient ionic conductivity this also indicates sufficient electronic conductivity, likely because the inserted Na ions and associated doping lead to a better electronic conductivity of the electrode. Similar effects have been reported on lithiation of Si,[25,26] and theoretical studies on Na ion insertion in Si based materials.[14,16]

To obtain insight in the equilibrium potentials during sodiation and desodiation the galvanostatic intermittent titration technique (GITT) is utilized. Current pulses of 20 mA g^{-1} for a 5 min duration are applied, with a relaxation period of 25 min in between in which the potential has time to relax in the direction of equilibrium. GITT (Figure 2e) shows a capacity of 771 mAh g^{-1} (i.e., $Na_{0.81}Si$) for Si during sodium insertion and a capacity of 360 mAh g^{-1} (i.e., $Na_{0.38}Si$) upon sodium extraction.

Figure 2e gives an indication of the overpotentials during cycling as well. Lower overpotentials are observed at lower voltage; whereas a relatively large overpotential up to ≈0.3 V can be observed when the voltage is above 1.0 V. A higher Na concentration apparently results in a better internal ionic and/or electronic conductivity.

The sloping lower voltage plateau (<0.5 V) for GITT sodiation, which is also observed in Figure 2b,d, may result from the coexistence of Si and NaSi. The proposal is thus that sodiation occurs in a two-phase equilibrium reaction (1)

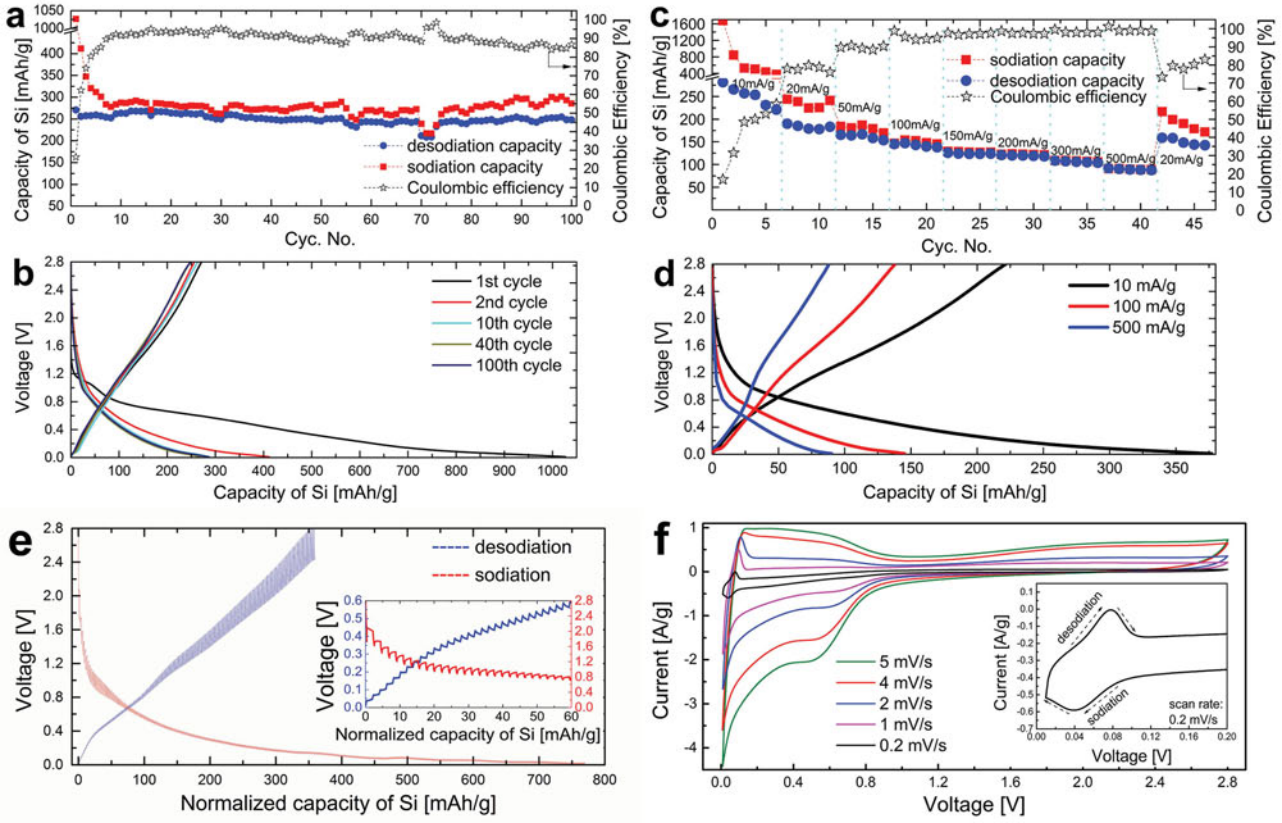

Figure 2. Electrochemical tests of Si NP electrodes: a) capacity retention and Coulombic efficiency, and b) charge/discharge voltage profiles at 20 mA g^{-1}, c) rate capability, d) voltage response of fifth cycle dis-/charge at different current rates, e) GITT de-/sodiation test (current pulses: 20 mA g^{-1} for 5 min during charge/discharge; relaxation for 25 min). GITT was carried out on a battery cell after cycling at 20 mA g^{-1} for five cycles. f) Cyclic voltammograms of Si NP electrode at different scan rates. Inset: cyclic voltammogram in the voltage range < 0.2 V at a scan rate of 0.2 mV s^{-1}.

$$x\mathrm{Na} + \mathrm{Si} = x\mathrm{NaSi} + (1-x)\mathrm{Si} \quad (1)$$

Cyclic voltammetry (CV) measurements were performed between 0.01 and 2.8 V at different scan rates. Figure 2f shows, at a scan rate of 0.2 mV s^{-1}, a distinct cathodic peak at 0.04 V attributed to the Na ion insertion into crystalline Si, which is extracted at 0.08 V during the anodic scan; whereas Na uptake in amorphous Si occurs at a higher and broader voltage range (<0.8 V). At increasing scan rates the potential peaks shift gradually to lower voltages for sodiation and higher potentials for desodiation, respectively, caused by the increasingly significant overpotentials. (More CV measurements on Si NP electrode and super P carbon electrode can be found in Figure S6, Supporting Information.)

To obtain more information about the sodiation mechanism of Si, XRD is conducted on an electrochemically cycled thicker (≈300 µm) pressed pellet electrode with the same composition as a slurry based electrode. The thicker electrode results in a better signal to noise ratio and avoids strong diffraction peaks from a Cu substrate. The pellet electrode is sodiated at 10 mA g^{-1} and a capacity of 736 mAh g^{-1} is achieved from this process. For the as-prepared and sodiated electrode a reflection mode XRD pattern was obtained under Ar atmosphere from the side of the electrode that has been in contact with the electrolyte, as is shown in **Figure 3**a,b. The peaks of crystalline Si are strongly reduced in the initially sodiated electrode, demonstrating the Na ion uptake and alloying process with crystalline Si. No distinct sharp extra peaks can be identified from the sodiated electrode. A broad bump at lower 2θ (20°–30°) emerges when comparing with the pristine electrode. Since various Na—Si alloys with larger unit cells exist, a contribution of such type of material can be present, however, in view of the large integrated intensity and the relatively smaller loss of Si diffraction intensity most of this additional broad diffraction intensity has to be attributed to the formation of an SEI layer on top of the Si electrode.

The Rietveld refinement of the thick electrode before and after first sodiation is performed via general structure analysis system (GSAS) program by including crystalline Si (space group: Fd-3m). There is a negligible lattice parameter increase (0.0014 Å) of the Si after sodiation which may indicate that at most a negligible amount of Na will be inserted in the crystalline Si phase. The difference before and after sodiation is a small but distinct domain size reduction of the crystalline Si. The size decreases from avg. 20.9 to 18.7 nm calculated by the Scherrer equation using a Lorentzian broadening (L_x) as observed in Figure 3d. Such size reduction corresponds to a reduction of 28.4% in volume, and therefore in mass. The amount of crystalline Si visible also decreased, but to an extent of 62% in the Rietveld refinement. This larger peak intensity

ADVANCED ENERGY MATERIALS
www.advenergymat.de

www.MaterialsViews.com

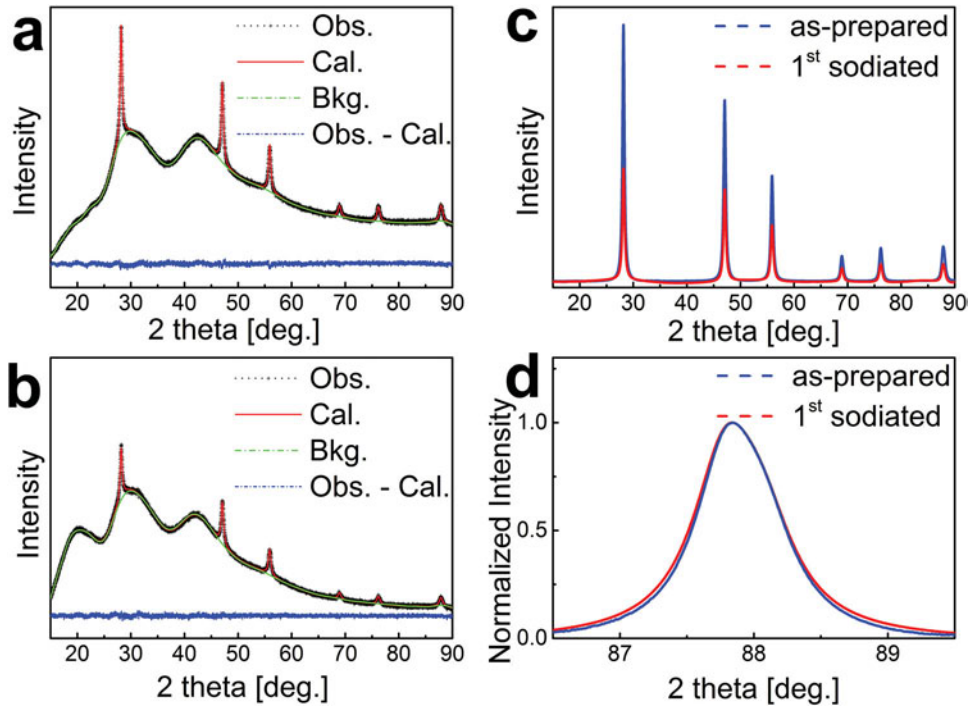

Figure 3. XRD patterns of the a) as-prepared and b) first cycle sodiated thick pellet electrode including Rietveld refinement. c) Refined XRD patterns of an Si NP pressed pellet electrode before and after initial sodiation, after subtraction of background. d) Lorentzian broadening (L_x) as observed at $2\theta = 87.9°$ before and after sodiation.

drop will be resulting from the absorption and scattering by the SEI layer on top of the electrode that weakens the X-ray diffraction intensity from the crystalline Si. We assume that the capacity for Na insertion may reach the composition Na_1Si in both amorphized Si on the surface of the crystalline particles and in the amorphous Si particles in the sample. Considering that the crystalline volume part reduces by 28.4% in the first cycle, the capacity contribution of crystalline and amorphous Si could be $954 \times 28.4\% = 271$ mAh g^{-1}, which fairly matches the reversible capacity observed for the whole sample, including the amorphous fraction. The Na storage in the amorphous Si therefore can consistently have a similar magnitude as in the crystalline fraction, which rapidly becomes amorphous upon sodiation. The further capacity loss during the first cycle must be due to the SEI formation. Also in view of the stable capacity retention for subsequent cycles in which crystalline Si is further converted to amorphous Si (Figure 1e and Figure S9, Supporting Information) there is no reason to assume a difference in Na insertion in amorphous or crystalline silicon.

The Na ion extraction occurs at different more strongly sloping voltages which may be indicating a desodiation reaction involving a solid solution of $Na_{1-x}Si$ with a Na content varying between 1 and 0, as is in reaction (2).

$$NaSi = Na_{1-x}Si + xNa \quad (2)$$

Such phases are also observed in high temperature synthesized NaSi and in $Na_{1-x}Si$ alloys and clathrate structures that are produced during high temperature extraction of Na from NaSi.[27,28] In view of the higher potentials during Na extraction, desodiation from NaSi proves to be more difficult than sodiation of Si.

In conclusion, nanoparticles containing both amorphous and crystalline Si, produced by ETPCVD, demonstrate an excellent reversible capacity of 279 mAh g^{-1} for Si at 10 mA g^{-1} and a capacity retention of 248 mA g^{-1} after 100 cycles at 20 mA g^{-1}. Significant reversible capacities can be achieved at high dis-/charge rates as well. We conclude that reversible electrochemical Na ion uptake in Si can be realized at room temperature. Nanoscaling benefits the Na insertion and extraction kinetics in Si although reversible Na uptake and release for the full theoretical capacity has not been reached. Initial amorphous and crystalline Si are performing an equally active role in the electrochemical sodiation. Coexistence of Si and NaSi may occur during Na insertion into amorphous Si and on the surface of the Si crystallites; while a solid solution desodiation reaction is evidenced when Na is being extracted. The observed first sizeable activity for reversible Na uptake may be applicable in a Na ion battery.

Experimental Section

Electrode Preparation: Electrodes were prepared by a conventional emulsion based process: a well-mixed slurry was prepared by mixing Si nanoparticles as obtained from ETPCVD, sodium carboxymethyl cellulose binder (NaCMC) (Aldrich), and Super P conductive carbon black in a weight ratio of 5:3:2 in deionized water; then the well-mixed slurry was cast onto Cu foil (Goodfellow) by doctor blading, followed by drying in a vacuum oven and pressing with a roller compressor for good electrical contact.

Electrochemistry: Half-cell Na ion batteries were tested with a counter electrode of Na metal foil, a borosilicate glass micro fiber separator (Whatman), and 1 M $NaClO_4$ dissolved in ethylene carbonate (EC)

and propylene carbonate (PC) (1:1 in volume) working electrolyte. Electrochemical performance was measured with a MACCOR 4600 battery cycler.

Supporting Information

Supporting Information is available from the Wiley Online Library or from the author.

Acknowledgements

This research was financially supported by A green Deal in Energy Materials (ADEM) grant funded by Dutch Ministry of Economic Affairs and ADEM industrial partners.

Received: July 16, 2015
Revised: September 19, 2015
Published online: November 9, 2015

[1] X. Fan, J. Mao, Y. Zhu, C. Luo, L. Suo, T. Gao, F. Han, S.-C. Liou, C. Wang, *Adv. Energy Mater.* **2015**, *5*, 1500174.
[2] H. Pan, X. Lu, X. Yu, Y.-S. Hu, H. Li, X.-Q. Yang, L. Chen, *Adv. Energy Mater.* **2013**, *3*, 1186.
[3] V. L. Chevrier, G. Ceder, *J. Electrochem. Soc.* **2011**, *158*, A1011.
[4] B. L. Ellis, L. F. Nazar, *Curr. Opin. Solid State Mater. Sci.* **2012**, *16*, 168.
[5] V. Palomares, P. Serras, I. Villaluenga, K. B. Hueso, J. Carretero-Gonzalez, T. Rojo, *Energy Environ. Sci.* **2012**, *5*, 5884.
[6] J. Ding, H. Wang, Z. Li, A. Kohandehghan, K. Cui, Z. Xu, B. Zahiri, X. Tan, E. M. Lotfabad, B. C. Olsen, D. Mitlin, *ACS Nano* **2013**, *7*, 11004.
[7] Y. Kim, Y. Kim, Y. Park, Y. N. Jo, Y.-J. Kim, N.-S. Choi, K. T. Lee, *Chem. Commun.* **2015**, *51*, 50.
[8] Y. Zhu, X. Han, Y. Xu, Y. Liu, S. Zheng, K. Xu, L. Hu, C. Wang, *ACS Nano* **2013**, *7*, 6378.
[9] D. Wu, X. Li, B. Xu, N. Twu, L. Liu, G. Ceder, *Energy Environ. Sci.* **2015**, *8*, 195.
[10] C. K. Chan, H. Peng, G. Liu, K. McIlwrath, X. F. Zhang, R. A. Huggins, Y. Cui, *Nat. Nanotechnol.* **2008**, *3*, 31.
[11] M.-H. Park, M. G. Kim, J. Joo, K. Kim, J. Kim, S. Ahn, Y. Cui, J. Cho, J. Cho, *Nano Lett.* **2009**, *9*, 3844.
[12] H. Wu, Y. Cui, *Nano Today* **2012**, *7*, 414.
[13] S. P. Ong, V. L. Chevrier, G. Hautier, A. Jain, C. Moore, S. Kim, X. Ma, G. Ceder, *Energy Environ. Sci.* **2011**, *4*, 3680.
[14] V. V. Kulish, O. I. Malyi, M.-F. Ng, Z. Chen, S. Manzhos, P. Wu, *Phys. Chem. Chem. Phys.* **2014**, *16*, 4260.
[15] H. Morito, T. Yamada, T. Ikeda, H. Yamane, *J. Alloys Compd.* **2009**, *480*, 723.
[16] I. M. Oleksandr, L. T. Teck, M. Sergei, *Appl. Phys. Express* **2013**, *6*, 027301.
[17] S. C. Jung, D. S. Jung, J. W. Choi, Y.-K. Han, *J. Phys. Chem. Lett.* **2014**, *5*, 1283.
[18] O. Malyi, V. V. Kulish, T. L. Tan, S. Manzhos, *Nano Energy* **2013**, *2*, 1149.
[19] F. Legrain, S. Manzhos, *J. Power Sources* **2015**, *274*, 65.
[20] F. Legrain, O. I. Malyi, S. Manzhos, *Comput. Mater. Sci.* **2014**, *94*, 214.
[21] L. D. Ellis, B. N. Wilkes, T. D. Hatchard, M. N. Obrovac, *J. Electrochem. Soc.* **2014**, *161*, A416.
[22] S. Komaba, Y. Matsuura, T. Ishikawa, N. Yabuuchi, W. Murata, S. Kuze, *Electrochem. Commun.* **2012**, *21*, 65.
[23] Y. Wang, H. Li, P. He, E. Hosono, H. Zhou, *Nanoscale* **2010**, *2*, 1294.
[24] P. G. Bruce, B. Scrosati, J. M. Tarascon, *Angew. Chem., Int. Ed.* **2008**, *47*, 2930.
[25] M. T. McDowell, Y. Cui, *Adv. Energy Mater.* **2011**, *1*, 894.
[26] E. Pollak, G. Salitra, V. Baranchugov, D. Aurbach, *J. Phys. Chem. C* **2007**, *111*, 11437.
[27] M. Pouchard, C. Cros, P. Hagenmuller, E. Reny, A. Ammar, M. Ménétrier, J.-M. Bassat, *Solid State Sci.* **2002**, *4*, 723.
[28] G. K. Ramachandran, J. Dong, J. Diefenbacher, J. Gryko, R. F. Marzke, O. F. Sankey, P. F. McMillan, *J. Solid State Chem.* **1999**, *145*, 716.

